

Acceleration and radiation of externally injected electrons in laser plasma wakefield driven by a Laguerre-Gaussian pulse^{*}

Zhongchen Shen(沈众辰)^{1,2} Min Chen(陈民)^{1,2†} Guobo Zhang(张国博)^{1,3} Ji Luo(罗辑)^{1,2} Suming Weng(翁苏明)^{1,2} Xiaohui Yuan(远晓辉)^{1,2} Feng Liu(刘峰)^{1,2}
Zhengming Sheng (盛政明)^{1,2,4}

¹ *Key Laboratory for Laser Plasmas (MoE) and School of Physics and Astronomy, Shanghai Jiao Tong University, Shanghai, 200240, China*

² *Collaborative Innovation Center of IFSA (CICIFSA), Shanghai Jiao Tong University, Shanghai 200240, China*

³ *College of Science, National University of Defense Technology, Changsha 410073, China*

⁴ *SUPA, Department of Physics, University of Strathclyde, Glasgow G4 0NG, UK*

By using three-dimensional particle-in-cell simulations externally injected electron beam acceleration and radiation in donut-like wakefields driven by a Laguerre-Gaussian pulse have been investigated. Studies show that during the acceleration process, the total charge and azimuthal momenta of electrons can be stably maintained for a few hundreds of micrometers distance. Electrons experience low frequency spiral rotation and high frequency betatron oscillation, which leads to synchrotron-like radiation. And the radiation spectrum is mainly determined by the electrons' betatron motion. The far field distribution of radiation intensity shows axial symmetry due to the uniform transverse injection and spiral rotation of electrons. Our studies suggest a new way to simultaneously generate hollow electron beam and radiation source from a compact laser plasma accelerator.

Keywords: laser plasma accelerator, particle-in-cell simulations, Laguerre-Gaussian pulse

PACS numbers: 52.38. Kd, 52.65. Rr, 42.55. -f

^{*} Project supported by the National Natural Science Foundation of China (Grant Nos. 11374209, 11374210, 11774227) and Major State Basic Research Development Program of China (2015CB859700).

[†] Corresponding author E-mail: minchen@sjtu.edu.cn

1. Introduction

About forty years ago, Tajima and Dawson proposed the concept of laser wakefield acceleration (LWFA) which shows great potential to realize compact accelerator with GeV/cm acceleration gradient.^[1-4] In the nonlinear regime of this scheme, when an ultraintense ultrashort laser pulse enters into an underdense plasma, the pondermotive force of the driver pulse expels background electrons forming an electron cavity composed of immobile ions in the center and dense electron current around the outside layer. This cavity structure moves behind the driver laser with a speed close to the laser group velocity.^[5,6] Such structure has both longitudinal accelerating and transverse focusing fields, which is a perfect acceleration cavity for electrons. Currently, electron acceleration with the maximum central energy of 4.2 GeV within an acceleration distance less than 10cm has been demonstrated in experiments.^[7] At the same time, compact radiation source studies based on LWFA have also attracted worldwide attentions.^[8-10] Radiations with photon energies from tens of eV to several MeV are generated from LWFA accelerated electrons interacting with external magnet or optical undulators.^[11-15] Besides these external undulators induced radiation, the accelerated electrons in wakefields also experience transverse oscillation due to the transverse focusing fields, which leads to betatron radiation. These radiation sources are achieved with relatively simple and compact setup and are suitable for wide applications.

Besides laser pulses with normal Gaussian mode, lasers with high order modes show more controllability on laser plasma interactions. Recently, intense laser pulses with Laguerre-Gaussian (LG) mode have been proposed,^[16] which provides the possibility to obtain electron beams and radiation sources with specific characters. High harmonics with angular momenta from laser solid target interaction and ring-shaped electron beam from wakefield acceleration by using ionization injection are observed in particle-in-cell (PIC) simulations when laser drivers with high order LG pulse are used.^[17-24] These researches extend the applications of laser driven secondary sources. In this paper, we expand our previous studies on wakefield

acceleration driven by LG pulses or similar type pulses by investigating the acceleration and radiation of externally injected electrons. ^[20,23,25] Our study aims to understand the acceleration and radiation characters of such beams in donut-like wakefields.

2. Wakefield driven by a LG-laser pulse

To investigate the electron acceleration in a donut-like wake driven by a laser pulse with fundamental mode, we performed three-dimensional (3D) PIC simulations by using the OSIRIS code. ^[26] In our studies, a linearly polarized LG laser with wave-length of 800 nm propagates along the x axis, the normalized vector potential of the driver laser with mode of $(l=1, p=0)$ has a form like $a(r, \xi) = a_0 r w_0^{-1} \exp[-r^2/w_0^2 - \xi^2/(c\tau)^2 + i\varphi]$. Here $\mathbf{a} = e\mathbf{A}/m_e c^2$ with \mathbf{A} is the amplitude of the laser vector potential, m_e and e are the electron mass and charge, respectively, c is the light speed in vacuum, $\xi = x - ct$ is the longitudinal coordinate in the moving window frame, $r = \sqrt{y^2 + z^2}$ is the radial distance from axis, and φ represents the azimuthal angle. Due to the limited computational resources, the simulations have scaled down to a relative small spatial-temporal size by using shorter laser duration and smaller laser focus. We take the peak amplitude $a_0 = 1.7$, the pulse duration $\tau = 6.6$ fs, and the radius of the focus spot $w_0 = 4 \mu\text{m}$. This small laser spot size gives a Rayleigh length of $63 \mu\text{m}$. To overcome laser diffraction, we used a pre-plasma channel with density profile of $n(r) = n_0 + \Delta n r^2/r_0^2$ to guide the propagation of laser pulse, where $\Delta n = n(r_0) - n(r=0)$ is the depth of the channel and r_0 represents the channel width. This kind of plasma channel has been proved to be very efficient to guide laser propagation. ^[2] In the simulation, the specific parameters of the channel are $n_0 = \Delta n = 8.71 \times 10^{18} \text{ cm}^{-3}$, $r_0 = 3.6 \mu\text{m}$, which increases the propagating distance to about $500 \mu\text{m}$. The simulation box with size of $30 \mu\text{m} \times 26 \mu\text{m} \times 26 \mu\text{m}$ is divided into $600 \times 208 \times 208$ cells. There are $2 \times 1 \times 1$ microscopic particles in each cell in typical 3D simulations.

Previous studies have shown that a donut like wake structure can be formed and a ring-shaped hollow electron beam can be injected and accelerated when a LG pulse and ionization injection are used. ^[20] The transverse ellipticity of the accelerated electron beam changes during the acceleration resulting from the electrons' residual azimuthal momenta obtained from the driver laser pulse and the focusing force of the wakefield. ^[20] To actively control such azimuthal rotation of the electron beam, we consider an externally injected electron beam here. The beam has an initial cuboid like spatial distribution with transverse size of $10 \mu\text{m} \times 10 \mu\text{m}$ and longitudinal

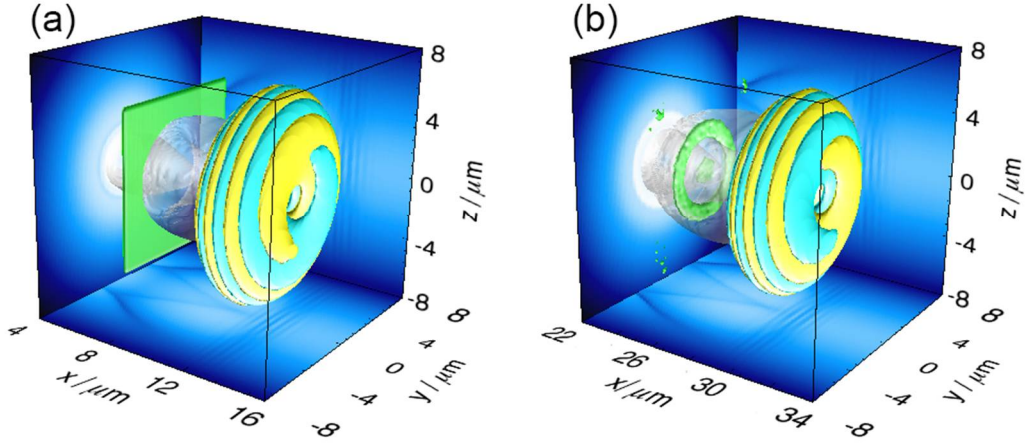


Fig. 1: (Color online) Spatial distribution of the laser fields, wakefields and electron beam density at instants of $t=57.42$ fs (a) and $t=114.84$ fs (b). The cyan-yellow colors represent the LG laser electric field. The olive and white colors represent the charge density of the externally injected electrons and the donut-like wake structure, respectively.

length of $0.1 \mu\text{m}$. The initial normalized transverse momenta have water-bag like distribution as $p_{y,z} \in [-1.23, 1.23]m_e c$ and the longitudinal momentum is fixed to be $p_x = 14.9m_e c$ to achieve the electrons injection. As we will see these nonzero transverse momenta introduce transverse spiral rotations to the injected electrons.

Figure 1 shows the spatial distribution snapshots of the laser fields, wakefields and externally injected electron beam at two different instants. The LG-pulse shows helical phase distributions with orbital angular momentum along the propagation direction, and the wake shows donut-like structure which can be clearly seen from the wake projection in the x - y plane. As one can see that a cuboid like externally injected electron beam has been used for the electron injection and after $17 \mu\text{m}$ long distance

of acceleration, the beam shows a hollow ring structure. Only the electrons initially locating inside the donut-like wakefield can be trapped and accelerated. The other electrons are transversely escaped from the wakefield. There are several small clouds of electrons staying at the outside of the ring in Fig. 1(b). However, after a further acceleration, these electrons are scattered in whole space completely. From the simulation, we found that nearly 7.64% of the externally injected electrons are trapped into the wake. The final shape of the accelerated electrons is similar as those ionization injected electrons shown in Ref. [20].

3. Dynamics of electrons accelerated in LG-pulse driven wakefields

Since the electrons injected here have an initial transverse momentum distribution ($p_{y,z} \in [-1.23, 1.23]m_e c$), besides longitudinal acceleration, they should also experience transverse rotation inside the donut-like wake. Unlike the ionization injected electrons only reserving the residual azimuthal momenta from the laser and piling up at two transverse ends of the wake, these externally injected electrons can make completely transversely spiral motions during the acceleration.

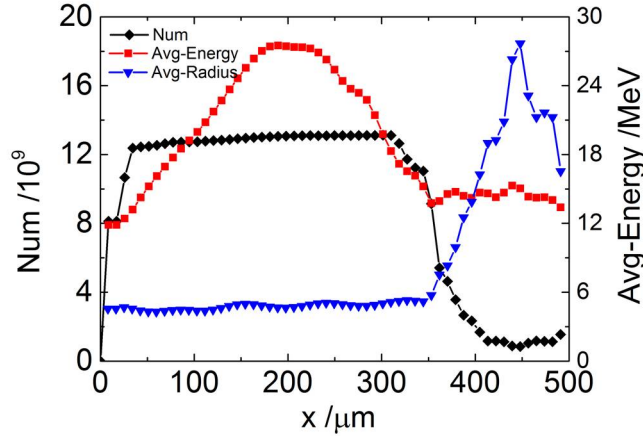


Fig. 2: (Color online) Evolution of the trapped and accelerated electron number (black line), the average electron energy (red line) and the average ring radius (blue line) along with the propagation distance.

In Fig. 2 we show the evolutions of the trapped electron number, the average electron energy and the radius of the electron ring along with the acceleration distance.

The radius of the electron ring is defined as $r_b = \sum_{i=1}^N \sqrt{(y_i - y_c)^2 + (z_i - z_c)^2} / N$,

where (y_i, z_i) are the transverse coordinates of each accelerated electrons, and (y_c, z_c) are the average center coordinates ($y_c = \sum_{i=1}^N y_i/N, z_c = \sum_{i=1}^N z_i/N$). One can see that the average electron radius is $r_b = 3 \mu\text{m}$, which is close to the transverse maximum intensity position of the LG laser. The evolution of the electron number shows that the ring-shaped electron beam can be continuously accelerated about $300\mu\text{m}$ in our simulation conditions. The average electron energy gradually increases from initial 8 MeV to 28 MeV within $189 \mu\text{m}$ acceleration distance. Later the energy descends because the electron beam enters into the dephasing phase, however, the beam is still inside the wake which can be clearly seen from the average radius

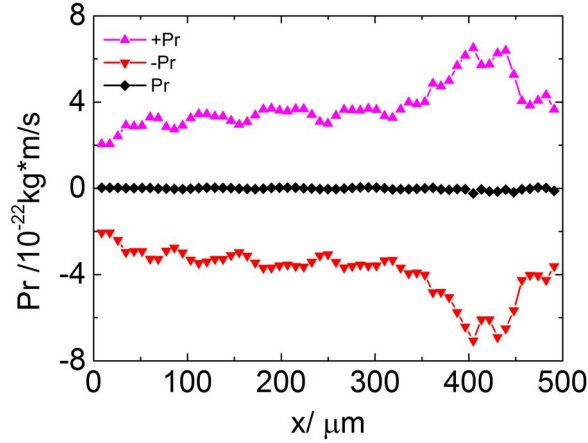


Fig. 3: (Color online) Evolution of the total azimuthal angular momenta of electrons. The upper pink triangles ($+Pr$) represent the positive azimuthal angular momenta (with the clockwise rotation), and the red lower triangles ($-Pr$) represent the negative azimuthal angular momenta. The central black dots represent the total azimuthal angular momenta (Pr).

evolution in Fig. 2. For a distance of $345\mu\text{m}$ the average radius keeps constant, which means these electrons are transversely trapped in the wakefield. However, after this distance, the radius of the electron beam rises sharply and the electron number decreases rapidly. Simulations show around this region the driver laser experiences a strong diffraction and the wake is not strong enough anymore to trap these electrons.

To see the transverse rotation of the electrons, we plot the azimuthal angular momenta of the electrons in Fig. 3. Both the positive and negative azimuthal angular momenta are shown. They are almost symmetrical and the ring-shaped electron beam has isotropic distribution, which is consistent with our expectation. On the one hand,

the initial transverse velocity distribution of the externally injected electrons is symmetrical in the transverse plane. On the other hand, the wakefield and the location where the electrons are injected are also symmetrical. The total azimuthal angular

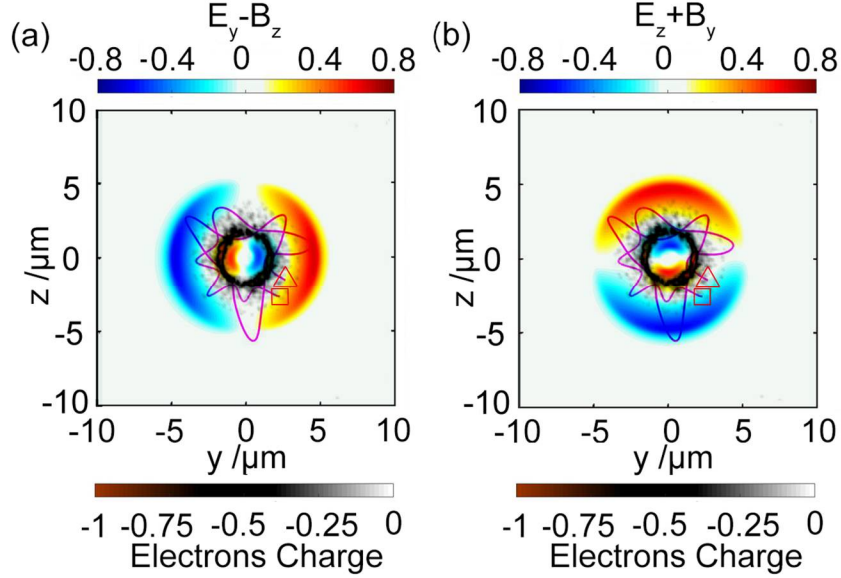


Fig. 4: (Color online) (a) Spatial distribution of fields combination ($E_y - B_z$) and externally injected electrons in the plane of $x = 189.5\mu m$. The trajectory projection in the $y - z$ plane of a typical accelerated electron is also shown. The rectangle and triangle mark the start and end positions of the trajectory, respectively. The up color bar shows the fields combination and the lower color bar shows the electron charge. (b) Spatial distribution of fields combination ($E_z + B_y$) and externally injected electrons at the same position.

momenta of the whole electron beam are close to zero. As one can see that between $0\mu m$ and $345\mu m$ the azimuthal angular momenta are nearly stable, and after this distance the angular momenta along each direction increase rapidly because these electrons begin to escape from the wake and only some electrons left are counted leading to different average angular momenta.

To investigate the dynamics of accelerated ring-shaped electrons, the transverse distribution of the wake fields, electron position and typical electron trajectory are shown in Fig. 4. A relatively special plane at $x = 189.5\mu m$ is selected since at this position the electrons have maximum energies and the electron number is relatively stable. As one can see from the fields and the electrons distributions, electrons are trapped in the donut-like wake and they feel radial forces making them rotate and

simultaneously oscillate inside the wake, which is the so-called spiral and betatron oscillation. A typical electron trajectory is shown by the colored line. From the trajectory the betatron motion with nine-period oscillations and spiral motion with two-cycle rotations are distinguishable in the whole acceleration process. The betatron motion is due to the transverse focusing fields of the wake and the rotation is due to the initial nonzero orbit angular momenta of the injected electrons. These trajectories are different from the ones of electrons in a normal Gaussian laser driven wakefield.

4. Radiation of accelerated rotating electrons in wakefields driven by LG-pulse

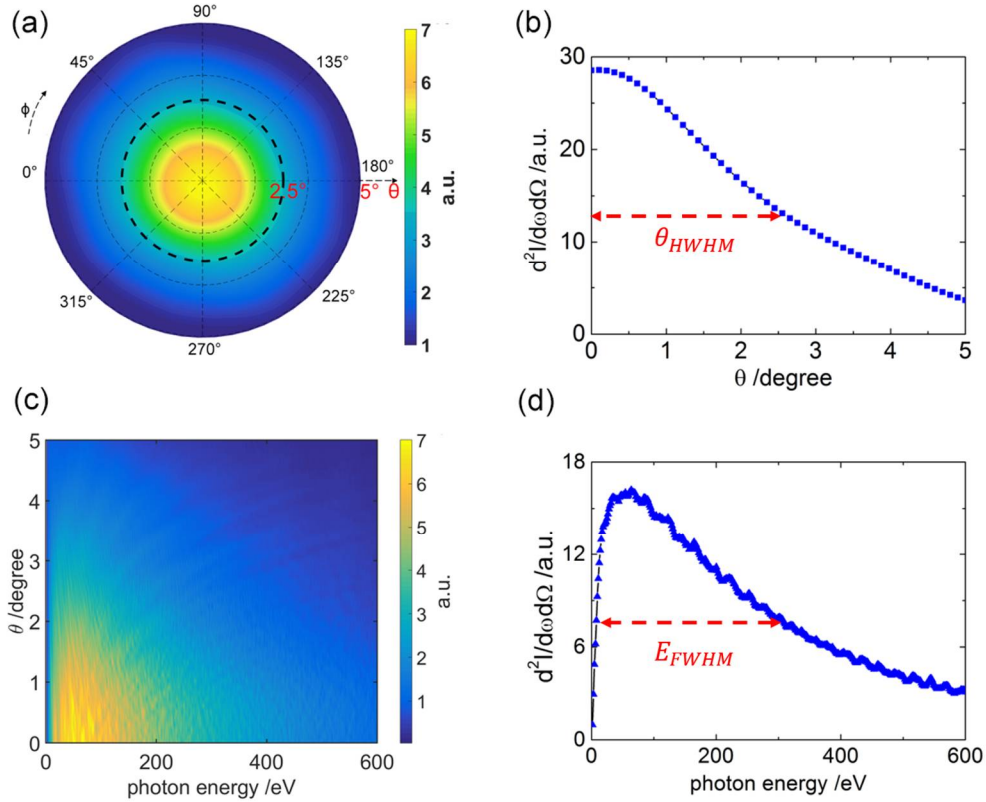


Fig.5 (Color online) (a) Intensity distribution of far field radiation within the range of $[0^\circ, 5^\circ]$ and $\phi \in [0^\circ, 360^\circ]$. (b) Radiation distribution as a function of the polar angle θ . (c) Radiation distribution in polar angle-energy space in the plane parallel to the laser polarization with $\phi = 0^\circ$. (d) The radiation spectrum along the laser propagation axis where the polar angle is $\theta = 0^\circ$ and the azimuthal angle is $\phi = 0^\circ$.

From the results shown above, we see besides the longitudinal acceleration,

electrons also make transverse oscillation and spiral rotation inside the wake. Accompanying with such kind of motion, electrons will radiate photons, which could be a useful light source. By using a post-processing code VDSR,^[27] we numerically study such radiation properties. The calculation is based on the integration of each particle's radiation along its trajectory:

$$\frac{d^2I}{d\omega d\Omega} = \frac{e^2}{4\pi^2 c} \left| \int_{-\infty}^{\infty} \frac{\mathbf{n} \times [(\mathbf{n} - \boldsymbol{\beta}) \times \dot{\boldsymbol{\beta}}]}{(1 - \boldsymbol{\beta} \cdot \mathbf{n})^2} e^{i\omega(t - \mathbf{n} \cdot \mathbf{r}(t)/c)} dt \right|^2 \quad (1)$$

And the code then calculates the beam's far field radiation by making incoherent summation of each electron's radiation. In our simulation totally 512 electrons' trajectories are randomly selected from all of the accelerated electrons to make radiation calculation. The correctness of the spectrum is proved by randomly selecting other group of particles whose spectrum is similar as this one.

A typical far field radiation distribution is shown in Fig. 5. As one knows usually the betatron radiation may show asymmetric far field intensity distributions if ionization injection is used or electrons have interacted with the driver pulse.^[28] The distribution is usually elongated along the laser polarization direction. In our simulation, Fig. 5(a) shows that the far field radiation intensity distribution has a quite good axial symmetry. This is related to uniformly transverse injection and spiral rotation of the electrons inside the donut-like wake. The half width at half maximum (HWHM) of the radiation distribution along the polar angle is about 2.6° as labeled in Fig. 5(b). In the simulation we find that the lowest relativistic factor of the electrons is $\gamma_{min} = 22.5$. According to the synchrotron radiation theory, the radiation should mainly propagate along an emission cone with open angle of $\theta < 1/\gamma \sim 2.5^\circ$, which is consistent with the simulation result.

The radiation spectrum is shown in Figs. 5(c) and 5(d). We find that the radiation peak is positioned at the photon energy about 50 eV and the FWHM of the spectrum is 269.2 eV. In our scheme, although the electrons make both betatron oscillation and spiral rotation, the former frequency ω_b is larger than the latter ω_r ($\omega_b/\omega_r \approx 4.5$), so the radiation spectrum is mainly determined by the betatron oscillation. The spiral rotation makes the radiation pattern more symmetric as we mentioned before. The

critical radiation photon energy of the betatron radiation can be evaluated by $E_p = \hbar\omega_c \approx 2\hbar\gamma^2 \left(\frac{2\pi c}{\lambda_\beta}\right)$ with $\lambda_\beta = \sqrt{2\gamma}\lambda_p$ and \hbar representing the reduced Planck constant. In our simulation the highest electron energy is about $\gamma_{max} = 54$, hence one expects $E_p = 57 \text{ eV}$ according to the formula given above. This is close to the peak photon energy ($\sim 50 \text{ eV}$) observed from the simulation with VDSR.

5. Summary

In summary, the acceleration and radiation of externally injected electrons in wakefields driven by a Laguerre-Gaussian pulse have been studied by computational simulations. The donut-like wakefield can not only longitudinally accelerate the ring-shaped electron beam, but also drive electrons to simultaneously rotate and do betatron oscillations in the wake. The electrons can generate radiation during spiral acceleration and betatron oscillation. The radiation spectrum is mainly determined by the high frequency betatron oscillation. The spiral rotation makes the far field radiation distribution show axial symmetry. Comparing with other wakefield based betatron radiation schemes due to self-injected and ionization injected electrons, the externally injected electrons can be easily controlled by tuning the beam injection angle and momentum. The donut like wake driven by the LG pulse just provides acceleration and radiation cavity to make both spiral rotation and betatron motion possible. Through this, one can obtain controllable far-field radiation pattern. In further, the combination of such simultaneous hollow electron beam and relatively uniform radiation source may have potential applications in some pump-probe studies.

[29]

We should point out that, due to the limited computational resources, the 3D simulations conducted here have been scaled down to a relatively small laser focus size which limits the acceleration length, so do the final electron beam energy and the radiated photon energy. In reality, one may use a larger laser focus and lower plasma density, which enable one to accelerate the electron beams to several hundreds of MeV and to extend the radiated photon energy to several keV level.

References

- [1] Tajima T, Dawson J M 1979 Phys. Rev. Lett. **43** 267
- [2] Esarey E, Schroeder C B, Leemans W P 2009 Rev. Mod. Phys. **81** 1229
- [3] Wang W T, Li W T, Liu J S, Zhang Z J, Qi R, Yu C H, Liu J Q, Fang M, Qin Z Y, Wang C, Xu Y, Wu F X, Leng Y X, Li R X and Xu Z Z 2016 Phys. Rev. Lett. **117** 124801
- [4] Zeng M, Chen M, Yu L L, Mori W B, Sheng Z M, Hidding B, Jaroszynski D A and Zhang J 2015 Phys. Rev. Lett. **114** 084801
- [5] Pukhov A, Meyer-ter-Vehn J 2002 J. Appl. Phys. B **74** 355–361
- [6] Lu W, Tzoufras M, Joshi C, Tsung F S, Mori W B, Vieira J, Fonseca R A and Silva L O 2007 Phys. Rev. ST Accel. Beams **10** 061301
- [7] Leemans W P, Gonsalves A J, Mao H S, Nakamura K, Benedetti C, Schroeder C B, Tóth C, Daniels J, Mittelberger D E, Bulanov S S, Vay J L, Geddes C G R and Esarey E 2014 Phys. Rev. Lett. **113** 245002
- [8] Corde S, Phuoc K T, Lambert G, Fitour R, Malka V, Rousse A, Beack A and Lefebvre E 2013 Rev. Mod. Phys. **85** 1
- [9] Chen M, Luo J, Li F Y, Liu F, Sheng Z M and Zhang J 2016 Light Sci. Appl. **5** e16015
- [10] Luo J, Chen M, Zeng M, Vieira J, Yu L L, Weng S M, Silva L O, Jaroszynski D A, Sheng Z M and Zhang J 2016 Sci. Rep. **6** 29101
- [11] Schlenvoigt H P, Haupt K, Debus A, Buddle F, Jäckel O, Pfotenhauer S, Schwoerer H, Rohwer E, Gallacher J G, Brunetti E, Shanks R P, Wiggins S M and Jaroszynski D A 2008 Nat. Phys. **4** 130–133
- [12] Fuchs M, Weingartner R, Popp A, Major Z, Becker S, Osterhoff J, Cortrie I, Zeitler B, Hörlein R, Tsakiris G D, Schramm U, Rowlands-Rees T P, Hooker S M, Habs D, Krausz F, Karsch S and Grüner F 2009 Nat. Phys. **5** 826–829
- [13] Phuoc K T, Corde S, Thaury C, Malka V, Tafzi A, Goddet J P, Shah R C, Sebban S and Rousse A 2012 Nat. Photonics **6** 308–311
- [14] Cipiccia S, Islam M R, Ersfeld B et al 2011 Nat Phys **7** 867–871
- [15] Wenchao Yan, Colton Fruhling, Grigory Golovin, Daniel Haden, Ji Luo, Ping Zhang, Baozhen Zhao, Jun Zhang, Cheng Liu, Min Chen, Shouyuan Chen, Sudeep Banerjee and Donald Umstadter, 2017 Nat. Photonics DOI:10.1038/NPHOTON.2017.100
- [16] Shi Y, Shen B F, L. Zhang L G, Zhang X M, Wang W P and Xu Z Z 2014 Phys. Rev. Lett. **112** 235001
- [17] Leblanc A, Denoëud A, Chopineau L, Mennerat G, Martin P and Quéré F 2017 Nat. Phys. **13** 440

-
- [18] Denoeud A, Chopineau L, Leblanc A and Quéré F 2017 Phys. Rev. Lett. **118** 033902
- [19] Zhang X M, Shen B F, Shi Y, Wang X F, Zhang L G, Wang W P, Xu J C, Yi L Q and Xu Z Z 2015 Phys. Rev. Lett. **114** 173901
- [20] Zhang G B, Chen M, C. B. Schroeder C B, Luo J, Zeng M, Li F Y, Yu L L, Weng S M, Ma Y Y, Yu T P, Sheng Z M and Esarey E 2016 Physics of Plasmas **23** 033114
- [21] Chen M, Sheng Z M, Ma Y Y and Zhang J 2006 J. Appl. Phys. **99** 056109
- [22] Chen M, Esarey E, Schoreder C B, Geddes C G R and Leemans W P 2012 Phys. Plasmas, **19** 033101
- [23] Zhang G B, Chen M, Luo J, Zeng M, Yuan T, Yu J Y, Ma Y Y, Yu T P, Yu L L, Weng S M and Sheng Z M 2016 J. Appl. Phys. **119** 103101
- [24] Vieira J and Mendonca J T 2014 Phys. Rev. Lett. **112** 215001
- [25] Yu L L, Schroeder C B, Li F Y, Benedetti C, Chen M, Weng S M, Sheng Z M and Esarey E 2014 Phys. Plasmas **21** 120702
- [26] Fonseca R A, Silva L O, Tsung F S, Decyk V K, Lu W, Ren C, Mori W B, Deng S, Lee S, Katsouleas T and Adam J C 2002 Lect. Notes Comput. Sci. Eng. **2331** 342
- [27] Chen M, Esarey E, Geddes C G R, Schroeder C B, Plateau G R, Bulanov S S, Rykovanov S and Leemans W P 2013 Phys. Rev. ST Accel. Beams **16** 030701
- [28] Döpp A, Mahieu A B, Lifschitz A, Thauray C, Doche A, Guillaume E, Grittani G, Lundh O, Hansson M, Gautier J, Kozlova M, Goddet J P, Rousseau P, Tafzi A, Malka V, Rousse A, Corde S and Phuoc K T 2017 Light: Science & Applications **6**, e17086; doi: 10.1038/lsa.2017.86
- [29] Yan W C, Chen L M, Li D Z, Zhang L, Hafz N A M, Dunn J, Ma Y, Huang K, Su L N, Chen M, Sheng Z M and Zhang J 2014 Proc. Natl. Acad. Sci. USA **111** 5825-5830